2018 NDIA GROUND VEHICLE SYSTEMS ENGINEERING AND TECHNOLOGY SYMPOSIUM
MATERIALS & ADVANCED MANUFACTURING (M&AM) TECHNICAL SESSION
AUGUST 7-9, 2018 – NOVI, MICHIGAN

USE OF CORROSION PRODUCT FOR DIGITAL IMAGE CORRELATION MEASUREMENTS

Bernard Sia
TARDEC
Warren, MI

ABSTRACT

This paper describes the results of work performed to assess the use of corrosion product for Digital Image Correlation (DIC) measurements. DIC was recently evaluated for its capability to measure contour, strain and deflection of metals using the corrosion product instead of a painted speckle pattern. The DIC system, consisting of two cameras with zoom lenses, was set up at an angle to the specimen, enabling both cameras to image multiple sides of a specimen simultaneously. This provides a more direct measurement of in-plane and out-of-plane deformation and strains. Aluminum and steel dogbones were placed in a salt spray chamber for up to 10 days. Contour measurements were then taken at various evaluation settings as an initial assessment of the use of the corrosion product for DIC measurements. Multiple tensile tests were then performed to assess the capability of using corrosion product for strain and deflection measurements while a material is under applied load. System bias and deviation was determined using static images taken of the corroded dogbones. Test results and analysis are presented in detail in this paper, as well as conclusions drawn as a result of these tests.

INTRODUCTION

Corrosion is the deterioration of a material as a result of chemical reactions between it and its surrounding environment. Corrosion's effect may be severe, both from a safety and economic standpoint. Therefore, it is necessary to understand the effects corrosion has on the performance of a material, specifically its mechanical properties. While techniques exist to measure the extent of corrosion, these measurements do not directly translate to an effect on a material's mechanical behavior. Alternative methods are needed to study this effect, and digital image correlation (DIC), a full-field, non-contact optical measurement technique, is one viable alternative due to its relative insensitivity to environmental interruptions and large measurement range, enabling it to measure both large and small effects.

DIC depends on adequate light intensity variation to ensure accurate matching between images taken for the measurement. This is normally obtained through the painting of a speckle pattern on the surface being measured. While speckle patterns can easily be painted in a laboratory environment, speckle patterns may not easily be painted in a field environment for various reasons, including inadequate access to the location of interest. Therefore, a need also exists to assess the capability of using natural speckle patterns, specifically the corrosion product, for DIC measurements.

An assessment was performed to examine the use of corrosion product instead of a painted speckle pattern for digital image correlation (DIC) measurements and assess the effect corrosion has on the properties of a material, specifically 6061 aluminum and A36 steel. This assessment was performed using a DIC setup which is capable of directly measuring in-plane and out-of-plane effects simultaneously. Section 2 of this paper provides an overview of digital image correlation, while Section 3 describes the alternative DIC setup used in this assessment. Sections 4 and 5 describe the test samples and experimental setup, while Sections 6-8 discuss the procedure and results of testing performed to examine the use of the corrosion product for DIC measurements and the effect of corrosion on the properties of 6061 aluminum and A36 steel. Section 9 summarizes the findings of the assessment.

SECTION 2: DIGITAL IMAGE CORRELATION OVERVIEW

Digital Image Correlation (DIC), first proposed by Peters and Ranson [1-2], is a whole field, non-contact optical measurement technique which operates under the principle of tracking the movement of multiple points using images taken before and after an object is deformed. The technique assumes that there is a direct correspondence between movement of points in the images and movement of points on the object. DIC is capable of measuring displacement, strain, and contour and has been used for measurements for a variety of applications, including material characterization [3-9] and blast loading [10-11]. 3-Dimensional (3-D) DIC, the schematic of which is shown in Figure 1, uses two or more cameras to enable an object's contour and out-of-plane displacement to be measured, in addition to in-plane displacement.

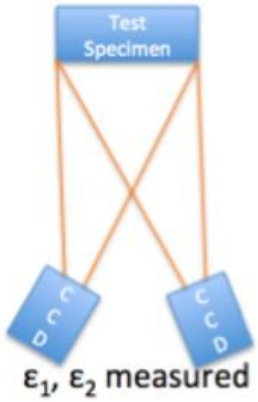

Figure 1: Traditional 3-D DIC Setup

DIC uses a correlation algorithm to track the grey value pattern in subsets, or areas of points, from images taken before and after an object is deformed. Two such algorithms are known as cross-correlation and normalized correlation and are shown in Equations (1) and (2), respectively.

$$c(u,v) = \sum_{x=-n}^{n} \sum_{y=-n}^{n} I_1(x,y) I_2(x+u, y+v) \tag{1}$$

$$c'(u,v) = \frac{\sum_x \sum_y I_1(x,y) I_2(x+u,y+v)}{\sqrt{\sum_x \sum_y I_1^2(x,y) I_2^2(x+u,y+v)}} \tag{2}$$

In Equations (1) and (2), $I_1(x,y)$ represents the pixel intensity at point (x,y) in Image 1, and $I_2(x+u, y+v)$ is the pixel intensity at point (x+u, y+v) in Image 2. For cross-correlation, a maximum value of correlation coefficient c(u, v) corresponds to the point (x+u, y+v) which has the most similar pattern to that seen in Image 1 at point (x, y), while, for normalized correlation, the closer the correlation coefficient c'(u, v) is to 1, the more similar the two subsets are. Normalized correlation generally provides better performance due to its independence of scale and subsequent insensitivity to changes in image amplitude. Successful image correlation also depends on the application of a random pattern onto the test specimen to provide variation in the light intensity. This is normally done through the painting of a speckle pattern onto the object. Subset size is also important, and the selection of subset size is dependent on various factors, including pixel resolution and spray pattern quality [12].

Once the maximum value of c(u,v) or c'(u,v) is found, in-plane displacements u and v can be determined by comparing the reference image and deformed image. The displacement is then translated to strain using the Lagrangian strain tensor shown in Equation (3).

$$\epsilon_{ij} = \frac{1}{2}\left(\frac{\partial u_i}{\partial x_j} + \frac{\partial u_j}{\partial x_i} + \sum_{l=1}^{3} \frac{\partial u_l}{\partial x_i}\frac{\partial u_l}{\partial x_j}\right) \quad (3)$$

SECTION 3: DOUBLE SIDE DIGITAL IMAGE CORRELATION SETUP

A problem with the traditional DIC setup is that it is unable to measure all three strain components directly. The traditional DIC setup uses the assumption of volume conservation to calculate out-of-plane strains [13-15]. However, it was found in [16] that the volume conservation assumption is not valid once the material is in the plastic range. Accurate measurement of the thickness strain, whether the specimen is corroded or not, is required for multiple applications, including characterization of the full strain state of the specimen and determination of a material's Forming Limit Diagram and plastic strain ratio. Figure 2 shows an alternative setup, known as the Double Side DIC setup, which enables measurement of all three strain components directly, as well as measurement of multiple elastic and plastic material properties in a single test without requiring multiple measurement tools. Similar in principle to a setup used in [9], the Double Side DIC setup places the DIC system at approximately a 45-degree angle to the test specimen, enabling multiple surfaces to be viewed at the same time. The setup maintains similar imaging models to traditional 3-D DIC setups, thus allowing the same calibration and evaluation algorithms to be used. Figure 3 shows an example of a strain map of a test specimen using the Double Side DIC setup.

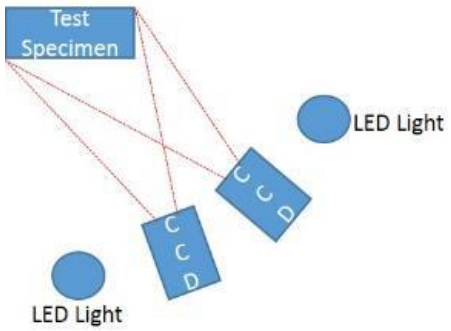

Figure 2: Double Side DIC Setup

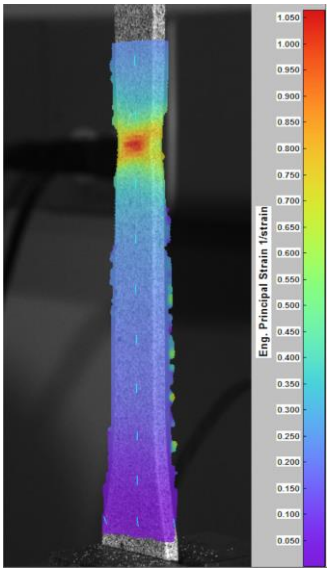

Figure 3: Strain Map Measured Using Double Side DIC Setup

Two important aspects for successful measurement using the Double Side DIC setup is the field of view (FOV) and depth of field (DOF). The FOV is especially important for measurement of the thickness surface, due to its small surface area relative to the front side. Equation (4) shows the equation for FOV with respect to the working distance *WD*, lens focal length *f* and camera chip size S_{chip}.

$$FOV = (\frac{WD}{f} - 1)S_{chip} \tag{4}$$

The FOV must be carefully designed to enable both the front and thickness side to be measured in the horizontal direction, while also enabling the entire gage length of the specimen in the vertical direction to be measured.

The DOF is an important consideration to enable the Double Side DIC setup to be able to measure the front and thickness surface simultaneously with good image quality. Careful consideration of the DOF is necessary because the Double Side DIC setup places the camera further away from some points of the specimen, while placing it closer to other points. The setup's DOF must be able to cover the full depth of the specimen when placed at an angle to it. Equation (5) shows the equation for DOF relative to the focus length *f*, aperture *N*, working distance *WD* and the diameter of the circle of confusion for a given image format *c*.

$$DOF = \frac{2Ncf^2WD^2}{f^4 - N^2c^2u^2} \tag{5}$$

Equations (4) and (5) can be used in conjunction with the specimen's dimensions, which will define the required DOF and FOV, to design the DIC system to enable successful measurement using the Double Side DIC setup.

SECTION 4: TEST SPECIMENS

6061 aluminum and A36 steel test specimens, fabricated in accordance with ASTM E8, were tested as part of this work. Prior to the start of testing, the specimens were placed in a salt spray chamber and exposed to

salt spray. The salt spray apparatus, operated in accordance to ASTM B117-111, used a salt solution of 5% Sodium Chloride in distilled water. All specimens were free of any flaws or preexisting damage and were not pre-strained before being placed in the salt spray chamber, and specimens were not coated with any surface coatings to allow for evaluation of the use of the corrosion product instead of a painted speckle pattern for measurements using DIC. Figures 4a and b show 6061 aluminum and A36 steel specimens after 192 hours of salt spray exposure. Specimens were exposed to salt spray for the following durations: 48 hours, 72 hours, 96 hours, 144 hours, 192 hours and 240 hours. Corrosion product, consisting of either a white surface product for aluminum or orange-brown product for the steel, was observed on all samples beginning at 48 hours of exposure.

a) 6061 Aluminum b) A36 Steel

Figure 4: Specimens After 192 Hours of Salt Spray Exposure

SECTION 5: EXPERIMENTAL SETUP

Figure 5 shows the experimental setup used for all tests performed in this work. Specimens were secured to a standard tensile test machine for contour measurements and testing under applied load. The Double Side DIC setup was used to measure all specimens tested in this work. The DIC system consisted of two high-resolution cameras and two 108 mm zoom lenses. LED lights were used to provide sufficient illumination to capture the full gage length of the specimen with good focus. An acquisition rate of 10 Hz was used for the DIC system, and the aperture of each lens was set to 8.

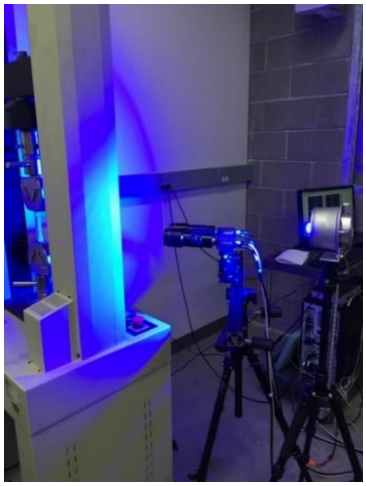

Figure 5: Experimental Setup

SECTION 6: CONTOUR MEASUREMENT ASSESSMENT USING CORROSION PRODUCT

The initial assessment of the use of the corrosion product for DIC measurements, consisting of a measurement of test specimen contour, was carried out using a total of 20 specimens, 5 specimens for each duration of salt spray exposure up to 192 hours. To measure the specimen's contour, images of a stationary specimen with no load applied were captured by the DIC system. The images were then evaluated using software. In the event an evaluation was unsuccessful, the images were reevaluated using a higher 3D Residuum limit value, which sets the maximum acceptable deviation between the pixel position found through image correlation and the back projected object point in the pixel [17], to assess if an increase in the limit enabled the evaluation to occur. An evaluation was considered successful if a contour map was generated by the software.

Overall, evaluation was successful for all aluminum and steel specimens using the corrosion product. Figures 6a and 6b show contour maps for aluminum and steel specimens exposed to salt spray for 192 hours. From this test series, it was found that specimens exposed to salt spray for longer amounts of time required higher 3D Residuum limit values to obtain successful correlation. The contour map quality also varied with the 3D Residuum limit, with higher limits producing higher quality contour maps, with fewer holes or discontinuities, due to the increased amount of deviation allowed between the pixel position found by the software during correlation and the back projected object point [17]. This results in more valid gridpoints found by the software and, subsequently, more available points that can be displayed.

Contour map quality was also found to vary with the material, as contour maps for the corroded aluminum specimens were generally of higher quality than that for the steel. The reduced quality of the steel contour maps is attributed partially to the exposing of base material as a result of corrosion product falling off of the specimen, but also to the larger areas of uniform color for the steel corrosion product. These uniform areas function in a similar fashion to large speckles, increasing the likelihood that subsets may lay entirely in a region containing this uniform area. As mentioned in [18], larger speckles increase the difficulty in locating the exact position at which the correlation coefficient is at a maximum, increasing the likelihood for higher errors due to the bias resulting from the occurrence of aliasing.

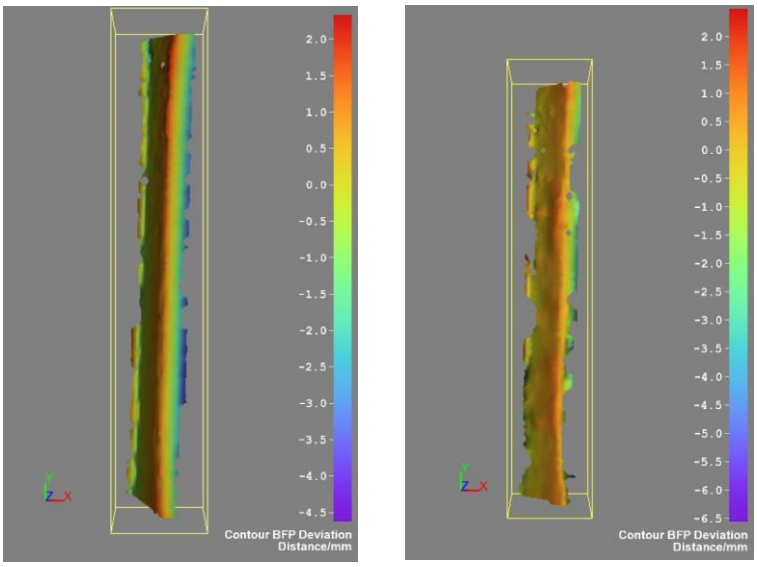

a) 6061 Aluminum b) A36 Steel

Figure 6: Contour Maps Measured Using Corrosion Product After 192 Hours Salt Spray Exposure

SECTION 7: BIAS/NOISE ASSESSMENT DIC USING CORROSION PRODUCT

An assessment of the bias and noise associated with DIC measurements using the corrosion product was also performed by capturing and evaluating multiple images of a stationary, undeformed specimen. In theory, deformation and strain for these specimens should equal zero for all DIC steps since no load is introduced to the specimen. Any non-zero measurement resulting from the evaluation of these stationary images provides an indication of the system's bias and noise, and knowledge of the system's bias and noise may be useful in the determination of overall DIC measurement uncertainty. The bias and noise of a DIC system corresponds to the mean and standard deviation of the deflection and strain measurements taken by the system [19-20].

Bias (mean) and noise (deviation) was evaluated for measurements on the front surface and thickness surface. Figures 7 and 8 show the results of this assessment for the aluminum specimens, while Figures 9 and 10 shows the results for the steel specimens. Overall, neither material showed a distinct trend between displacement bias and strain bias with exposure time for front surface measurement. Steel displacement and longitudinal strain deviation on the front side also does not show a specific trend with respect to exposure time, while steel transverse strain deviation exhibits a slight decreasing trend. Aluminum displacement deviation on the front surface also shows a specific trend, as x-displacement deviation increased and y-displacement deviation decreased with respect to exposure time, as does aluminum longitudinal strain deviation. For thickness surface measurement, steel displacement bias and deviation also did not show a specific trend with respect to exposure time. Some parameters, specifically longitudinal strain deviation, longitudinal strain bias, and y-displacement bias, behaved in a similar fashion to what was observed on the front surface for steel. Aluminum displacement deviation also showed a similar trend on the thickness surface to what was observed on the front surface, increasing with respect to exposure time for x-displacement deviation and decreasing for y-displacement deviation. Longitudinal strain bias and deviation on the thickness surface also showed slight increasing trends with exposure time, with deviation behaving similarly to the behavior observed for the front surface measurement. No other parameter exhibited any specific trend with respect to exposure time for the aluminum. Comparing front and thickness surface measurement magnitudes for the exposure durations used in this assessment, front surface bias and deviation magnitudes were generally higher than that for the thickness surface for the aluminum specimens. For the steel specimens, thickness surface magnitudes were generally higher than front surface measurements at 2 days exposure time, but gradually became lower than the front surface results as exposure time increased. Factors affecting the results of this assessment include the greater thickness of the steel corrosion product compared to the aluminum corrosion product and the greater uniformity of the steel corrosion product, which function in a similar fashion to large speckles. It is noted that further evaluation is needed to generalize the behavior observed in this assessment, as other variables which may affect the results, such as viewing size and aperture setting [21], were not considered in this assessment.

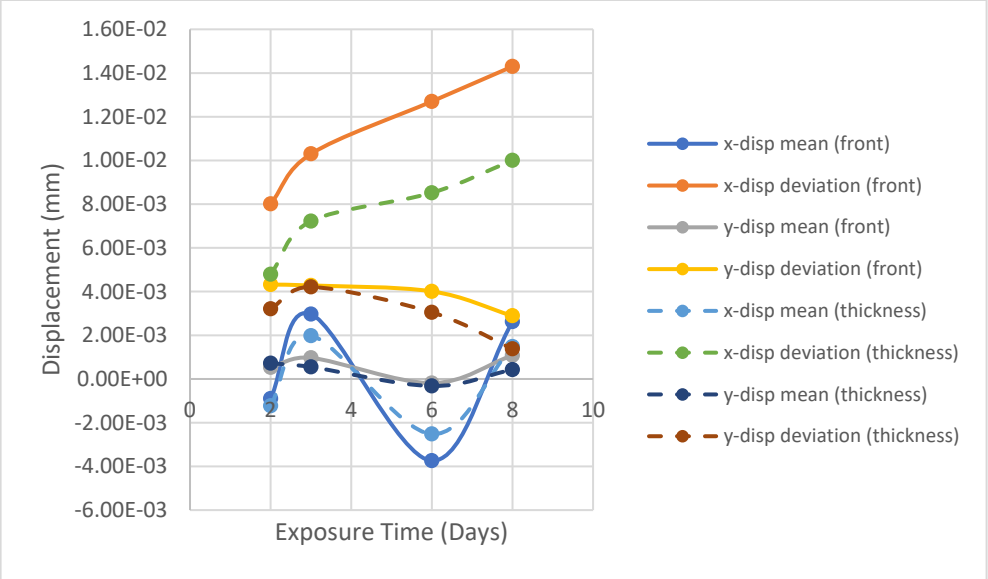

Figure 7: Aluminum Displacement Bias and Deviation for Various Salt Spray Exposure Times

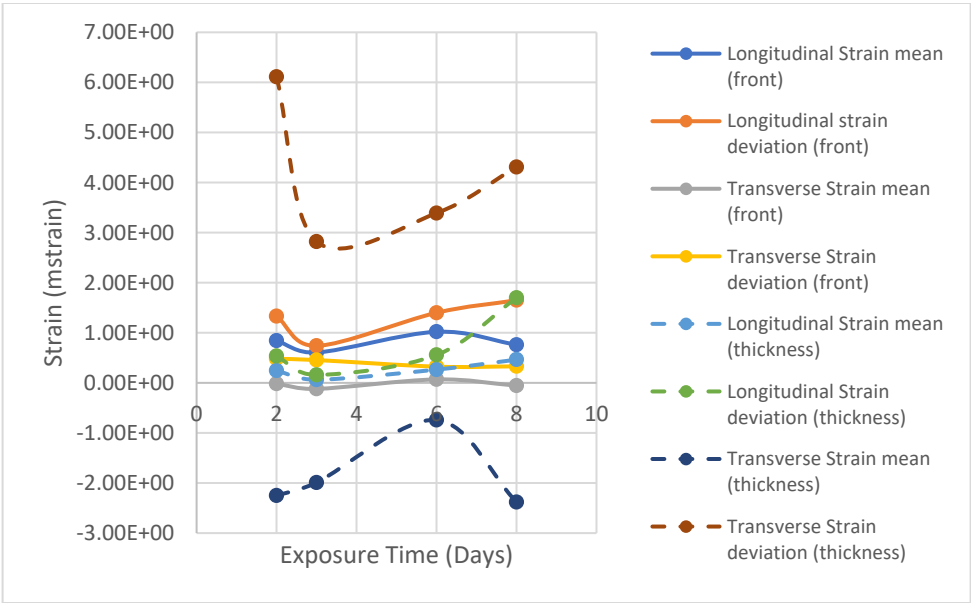

Figure 8: Aluminum Strain Bias and Deviation for Various Salt Spray Exposure Times

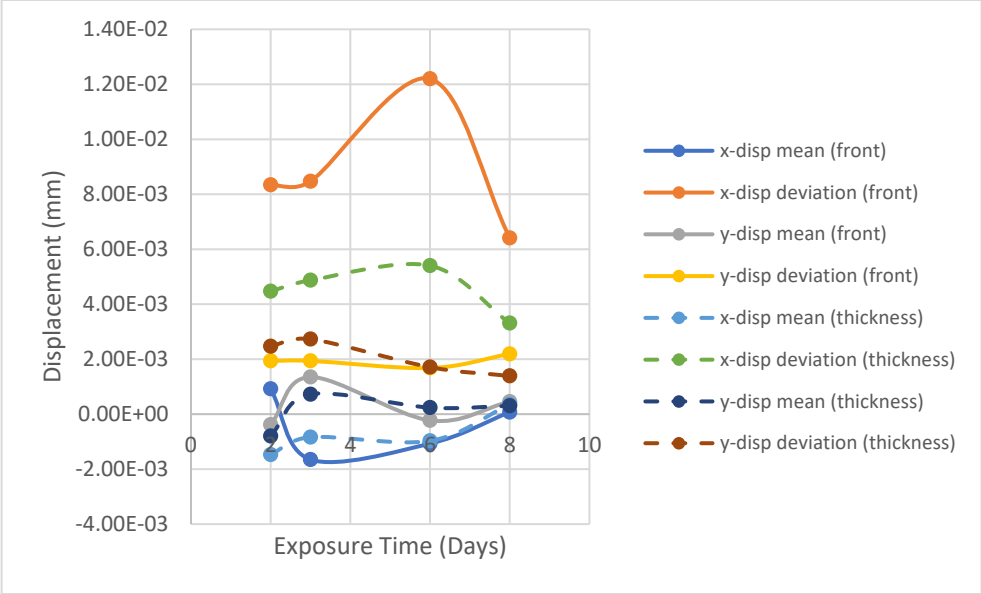

Figure 9: Steel Displacement Bias and Deviation for Various Salt Spray Exposure Times

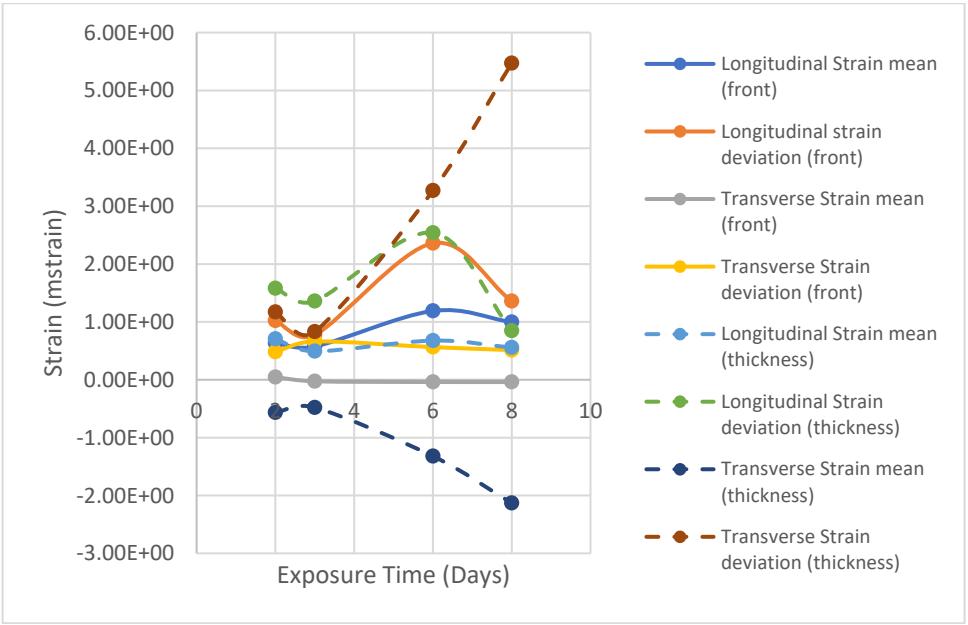

Figure 10: Steel Thickness Surface Bias and Deviation for Various Salt Spray Exposure Times

SECTION 8: TENSILE TEST OF CORRODED SPECIMENS

Tensile tests were also performed on the aluminum and steel specimens to assess the effect of salt spray exposure on various elastic, plastic and strain hardening properties of the material. All tensile tests were performed at a loading speed of 7.62 mm/min. A relatively slow loading speed was used to maximize the number of images taken of each specimen prior to failure and limit the potential for outside influences resulting

from higher loading speeds from affecting the test results. Due to the poor contour map quality obtained with the steel corrosion product compared to the aluminum corrosion product, as exhibited in Figure 6b, a painted speckle pattern was used for measurement of the steel specimens. Prior to the performance of the tensile tests, corrosion product was cleaned off of the steel specimens to expose the resulting damage from the corrosion exposure, and a speckle pattern, consisting of black speckles on a white background, was painted on the front and thickness surfaces of the specimen. Corrosion product, however, was not cleaned off of the aluminum specimens. Instead the corrosion product was used as the means of providing light intensity variation for the purpose of DIC measurements. Figure 9 shows a strain map of a corroded aluminum specimen just before specimen failure. Correlation was successful up to specimen failure for all corroded aluminum specimens using the corrosion product, with few holes in the strain map, further demonstrating the capability of using the corrosion product for DIC measurements of specimens under applied load.

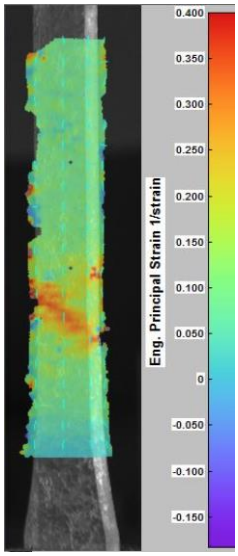

Figure 9: Corroded Aluminum Specimen Strain Map Just Before Failure

Tables 1 and 2 show the average results of the tensile tests for the corroded aluminum and steel specimens, respectively. For 6061 aluminum, the elastic properties were generally found to be constant with respect to exposure time, with the percent change in values from 2 days exposure time to 10 days exposure time ranging from 2 to 7 percent. Poisson's Ratio exhibited more variation compared to the other properties, with percent uncertainties ranging from 13 percent to 32 percent, but is considered to be constant with exposure time once uncertainty is considered. Aluminum plastic properties and strain hardening properties were also found to be generally constant with respect to exposure time, with percent change from 2 to 10 days exposure time ranging from 1 percent to 6 percent. It is noted that a few properties, such as longitudinal stiffness and ultimate load, exhibited sharper changes in value from 8 to 10 days exposure time compared to that seen at other durations. Further research is necessary to determine if this trend is followed at higher exposure times.

		Salt Spray Duration (Days)				
		2	3	6	8	10
Elastic Properties	Longitudinal Stiffness, E (MPa)	74,442 ± 820	73,059± 829	73,448± 1242	74,142± 1779	69,135± 2033
	Yield Strength, σ_y (MPa)	307 ± 1	307± 3	306± 3	303± 3	301± 1
	Poisson's Ratio	0.28 ± 0.08	0.30± 0.08	0.25± 0.08	0.32± 0.04	0.30± 0.04
	Resilience (MPa)	0.63 ± 0.01	0.64 ± 0.02	0.64 ± 0.02	0.61 ± 0.02	0.66± 0.02
Plastic Properties	Ultimate Load (N)	13,291±23	13,271± 32	13,275± 37	13,244± 51	12,939± 15
	Ultimate Strength (MPa)	333± 1	332± 2	331± 3	328± 3	321± 1
	Strain at Failure	0.17 ± 0.01	0.18 ± 0.01	0.18± 0.02	0.18 ± 0.01	0.17 ± 0.00
	Stress at Fracture (MPa)	295 ± 4	294 ± 2	300 ± 2	294 ± 2	276 ± 2
	Toughness (MPa)	54 ± 3	56 ± 2	57 ±5	58 ± 4	52 ± 1
	Plastic Strain Ratio	0.56 ± 0.17	0.56 ± 0.06	0.56 ± 0.14	0.64 ± 0.04	0.56 ± 0.05
Strain Hardening Properties	Strength Coefficient (MPa)	463 ± 2	459 ± 3	460 ± 4	457 ± 2	435 ± 1
	Strain Hardening Exponent	0.10 ± 0.0	0.10 ± 0.0	0.10 ± 0.0	0.10 ± 0.0	0.09 ± 0.0

Table 1: 6061 Aluminum Elastic, Plastic and Strain Hardening Properties at Various Salt Spray Exposure Times

		Salt Spray Duration (Days)				
		2	3	6	8	10
Elastic Properties	Longitudinal Stiffness, E (MPa)	218,572± 8004	243,486± 6486	254,856 ± 8029	242,083 ± 18,193	209,502 ± 6127
	Yield Strength, σ_y (MPa)	308 ± 3	314± 3	310± 3	305± 4	299± 7
	Poisson's Ratio	0.32 ± 0.05	0.32 ± 0.05	0.32 ± 0.07	0.32 ± 0.03	0.32 ± 0.04
	Resilience (MPa)	0.22 ± 0.01	0.20 ± 0.01	0.19 ± 0.01	0.20 ± 0.01	0.22 ± 0.01
Plastic Properties	Ultimate Load (N)	14,224 ± 52	14,328 ± 107	14,165 ± 62	14,070 ± 58	13,952 ±157
	Ultimate Strength (MPa)	395± 1	400± 3	393±2	388± 3	389± 3
	Strain at Failure	0.40 ± 0.01	0.36 ± 0.01	0.35 ± 0.02	0.40 ± 0.02	0.29 ± 0.03
	Stress at Fracture (MPa)	267 ± 5	285 ± 4	280 ± 5	266 ± 11	220 ± 34
	Toughness (MPa)	141 ± 4	129 ± 2	125 ± 8	138 ± 5	101 ± 8
	Plastic Strain Ratio	0.87 ± 0.05	0.91 ± 0.01	0.91 ± 0.01	0.87 ± 0.03	0.90 ± 0.05
Strain Hardening Properties	Strength Coefficient (MPa)	629 ± 3	639 ± 7	624 ± 3	620 ± 5	622 ± 3
	Strain Hardening Exponent	0.17 ± 0.00	0.17 ± 0.00	0.17 ± 0.00	0.17 ± 0.00	0.17 ± 0.00

Table 2: A36 Steel Elastic, Plastic and Strain Hardening Properties at Various Salt Spray Exposure Times

A36 steel properties generally exhibited more change that 6061 aluminum with respect to salt spray exposure time. Stiffness exhibited a slight overall decreasing trend with respect to exposure time for the exposure times assessed in this research, while A36 resilience, which was estimated using Equation 6 for both materials, stayed essentially constant for the exposure times assessed in this research. Some variability does exist in this data, and further research is needed to determine if this variability is attributed to corrosion or to other factors such as material processing.

$$Resilience = u_r \approx \frac{\sigma_y^2}{2E} \quad (6)$$

Yield strength gradually decreased in a linear fashion with increasing exposure time, while Poisson's Ratio essentially stayed constant, uncertainty taken into account. Ultimate load and strength showed a similar gradual and linear decrease to what was observed for the yield strength. Strain to failure and toughness both exhibited general decreasing trends with respect to exposure time, while plastic strain ratio generally remained constant. With respect to the strain hardening properties, strength coefficient showed a general decreasing trend with increased exposure time, while the strain hardening exponent remained constant.

The decreasing trend exhibited by the strain to failure and toughness appear to indicate that A36 steel is becoming more brittle as the exposure time increases. Failure surfaces were analyzed for a virgin A36 steel specimen and A36 steel specimen exposed to salt spray for 10 days to determine if a change occurs in the fracture surface. Figures 10 and 11 show the resulting failure surface for the virgin A36 specimen and corroded A36 specimen. As Figures 10 and 11 indicate, both specimens have a failure surface characteristic of a dimpled rupture, a type of ductile failure characterized by cuplike depressions. Figure 11 does not show any significant signs of granular fracture surfaces that are characteristic of brittle materials. Therefore, it is concluded that a change in the failure mode is not the underlying cause of the trend experienced by the A36 strain to failure and toughness. It is noted that material loss, as well as the level of pitting and surface damage, did increase with increasing exposure to salt spray. This material loss was non-uniform, resulting in variations in the cross-section along the length of the specimen. Areas of lower cross-section have less material to withstand the applied load, thus resulting in failure at lower stresses and, as a result, the observed decrease in the yield and ultimate strength, as well as the observed decreasing trend in strain to failure and toughness.

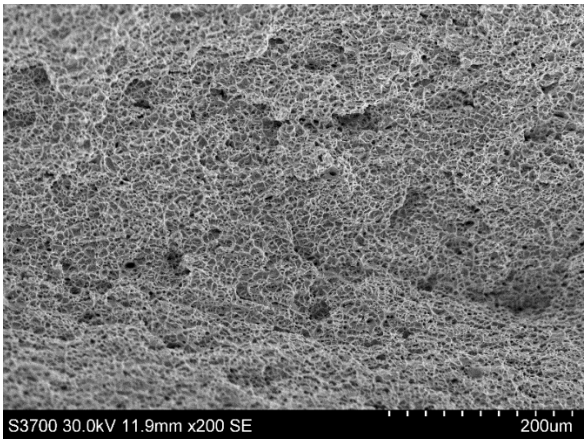

Figure 10: SEM Image of Virgin A36 Steel Fracture Surface Shows Failure due to Dimple Rupture

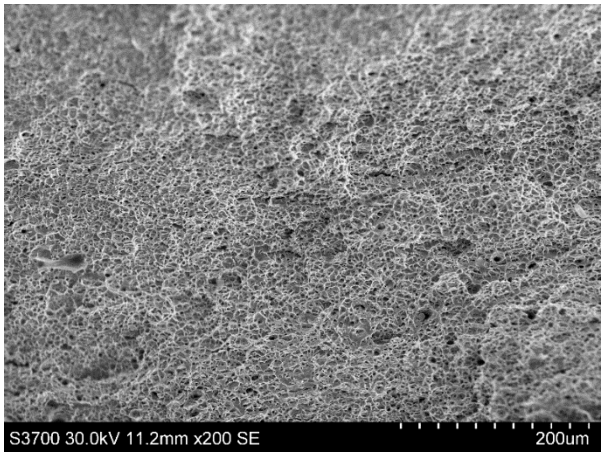

Figure 11: A36 Steel Exposed to 10 Days Salt Spray Exposure Shows Similar Fracture Surface to Virgin A36 Steel

SECTION 9: CONCLUSION

The use of the corrosion product resulting from exposure to salt spray was assessed for measurement of strain and deformation using a DIC system. The DIC system was set up to image multiple sides of a specimen simultaneously, providing a more direct measurement of in-plane and out-of-plane effects. Contour measurements were successfully taken, establishing the viability of using the corrosion product for DIC measurements and the utility of DIC for measurements of corroded equipment in the field. System bias and deviation using the corrosion product was also assessed, providing an understanding of the potential error associated with such a measurement. Tensile tests performed on corroded 6061 aluminum specimens demonstrated the capability of using the corrosion product to measure strain and deformation up to the point of specimen failure using DIC. The effect of corrosion exposure on the elastic, plastic and strain hardening properties of 6061 aluminum and A36 steel was also assessed, thus giving insight into the effect corrosion has on the performance of these materials. Steel elastic and plastic properties were generally found to be more affected by exposure to salt spray than aluminum properties. The strength coefficient changed slightly for both materials with respect to exposure duration, while the strain hardening exponent was found to be insensitive to corrosion exposure. Areas of future work resulting from the research described in this paper include assessing the effect of corrosion on the mechanical behavior of materials coated with anti-corrosive coatings, as well as assessing the measurement capability of DIC using a painted speckle pattern and corrosion product at the same time.

REFERENCES

[1] Wang, Y., & Cuitiño, A. M. (2002). Full-field measurements of heterogeneous deformation patterns on polymeric foams using digital image correlation. *International Journal of Solids and Structures*, *39*(13), 3777-3796.

[2] Peters, W. H., & Ranson, W. F. (1982). Digital imaging techniques in experimental stress analysis. *Optical engineering*, *21*(3), 213427-213427.

[3] Wattrisse, B., Chrysochoos, A., Muracciole, J. M., & Némoz-Gaillard, M. (2001). Analysis of strain localization during tensile tests by digital image correlation. *Experimental Mechanics*, *41*(1), 29-39.

[4] Tung, S. H., Shih, M. H., & Kuo, J. C. (2010). Application of digital image correlation for anisotropic plastic deformation during tension testing. *Optics and Lasers in Engineering*, *48*(5), 636-641.
[5] Jiang, J., Wang, H., & Gu, J. (2013). *Constitutive Model of Ti40 Alloy Sheet Based on DIC Measurement* (No. 2013-01-1427). SAE Technical Paper.
[6] Périé, J. N., Leclerc, H., Roux, S., & Hild, F. (2009). Digital image correlation and biaxial test on composite material for anisotropic damage law identification. *International Journal of Solids and Structures*, *46*(11), 2388-2396.
[7] Laurin, F., Charrier, J. S., Lévêque, D., Maire, J. F., Mavel, A., & Nunez, P. (2012). Determination of the properties of composite materials thanks to digital image correlation measurements. *Procedia IUTAM*, *4*, 106-115.
[8] Périé, J. N., Calloch, S., Cluzel, C., & Hild, F. (2002). Analysis of a multiaxial test on a C/C composite by using digital image correlation and a damage model. *Experimental Mechanics*, *42*(3), 318-328.
[9] Grytten, F., Daiyan, H., Polanco-Loria, M., & Dumoulin, S. (2009). Use of digital image correlation to measure large-strain tensile properties of ductile thermoplastics. *Polymer Testing*, *28*(6), 653-660.
[10] Tiwari, V., Sutton, M. A., McNeill, S. R., Xu, S., Deng, X., Fourney, W. L., & Bretall, D. (2009). Application of 3D image correlation for full-field transient plate deformation measurements during blast loading. *International Journal of Impact Engineering*, *36*(6), 862-874.
[11] Reu, P. L., & Miller, T. J. (2008). The application of high-speed digital image correlation. *The Journal of Strain Analysis for Engineering Design*, *43*(8), 673-688.
[12] Lecompte, D., Smits, A., Bossuyt, S., Sol, H., Vantomme, J., Van Hemelrijck, D., & Habraken, A. M. (2006). Quality assessment of speckle patterns for digital image correlation. *Optics and lasers in Engineering*, *44*(11), 1132-1145.
[13] Hoffmann, H., & Vogl, C. (2003). Determination of true stress-strain-curves and normal anisotropy in tensile tests with optical strain measurement. *CIRP Annals-Manufacturing Technology*, *52*(1), 217-220.
[14] Rossi, M., Broggiato, G. B., & Papalini, S. (2008). Application of digital image correlation to the study of planar anisotropy of sheet metals at large strains. *Meccanica*, *43*(2), 185-199.
[15] Tay, C. J., Quan, C., Huang, Y. H., & Fu, Y. (2005). Digital image correlation for whole field out-of-plane displacement measurement using a single camera. *Optics Communications*, *251*(1), 23-36.
[16] Xie, X., Li, J., Sia, B., Bai, T., Siebert, T. and Yang, L., 2017. An experimental validation of volume conservation assumption for aluminum alloy sheet metal using digital image correlation method. The Journal of Strain Analysis for Engineering Design, 52(1), pp.24-29.
[17] Dantec Dynamics. (2016). *Istra 4D Software Manual Q-4xx System*. Skovlunde, Denmark: Author.
[18] Lecompte, D., Bossuyt, S., Cooreman, S., Sol, H., & Vantomme, J. (2007). Study and generation of optimal speckle patterns for DIC. In *Proceedings of the annual conference and exposition on experimental and applied mechanics* (Vol. 3, pp. 1643-1649).
[19] Ke, X. D., Schreier, H. W., Sutton, M. A., & Wang, Y. Q. (2011). Error assessment in stereo-based deformation measurements. *Experimental mechanics*, 51(4), 423-441.
[20] Robert, L., Nazaret, F., Cutard, T., & Orteu, J. J. (2007). Use of 3-D digital image correlation to characterize the mechanical behavior of a fiber reinforced refractory castable. *Experimental Mechanics*, *47*(6), 761-773.
[21] Reu, P. L., Sweatt, W., Miller, T., & Fleming, D. (2015). Camera system resolution and its influence on digital image correlation. *Experimental Mechanics*, *55*(1), 9-25.